Materials Characterization and Spectroscopy for a Methane Abatement Catalyst

by

Mollie Wilkinson

S.B., Massachusetts Institute of Technology (2022)

Submitted to the Department of Civil and Environmental Engineering
in partial fulfillment of the requirements for the degree of

Master of Engineering in Civil and Environmental Engineering

at the

MASSACHUSETTS INSTITUTE OF TECHNOLOGY

June 2023

Author
Mollie Wilkinson
Department of Civil and Environmental Engineering
May 12, 2023

Certified by
Desiree Plata
Gilbert W. Winslow (1937) Career Development Professor in Civil Engineering
Thesis Supervisor

Accepted by
Colette L. Heald
Professor of Civil and Environmental Engineering
Chair, Graduate Program Committee

Materials Characterization and Spectroscopy for a Methane Abatement Catalyst

by

Mollie Wilkinson

Submitted to the Department of Civil and Environmental Engineering
on May 12, 2023, in partial fulfillment of the
requirements for the degree of
Master of Engineering in Civil and Environmental Engineering

Abstract

Methane is the second-most emitted greenhouse gas after carbon dioxide, and it is significantly more powerful as a short-term warmer, making it a valuable target for climate change mitigation efforts. Zeolites are earth-abundant minerals common in catalysis for their low price combined with high conversion and throughput potential. This study evaluates a specific copper-zeolite (mordenite) methane oxidation catalyst for long-term durability and potential performance at 400 and 950 °C. Using materials characterization and spectroscopy techniques including scanning-electron microscopy (SEM), energy-dispersive X-ray spectroscopy (EDS), Brunauer-Emmett-Teller analysis (BET), differential scanning calorimetry (DSC), and X-ray diffraction (XRD), chemical and structural changes are tracked, identified, and assessed over the course of three months. Samples treated at 400 °C show no major structural or chemical changes in the catalyst, while samples treated at 950 °C show gradual transformation into a nonporous quartz-mullite-cristobalite mixture. This suggests indefinite catalyst stability at the former temperature and progressive catalyst degradation at the latter temperature, providing plausible long-term operation conditions and peak temporary conditions for this method of methane abatement.

Thesis Supervisor: Desiree Plata
Title: Gilbert W. Winslow (1937) Career Development Professor in Civil Engineering

Acknowledgments

First and foremost, I would like to express my deepest gratitude to my research advisor and mentor, Desiree Plata. Desiree has been instrumental to my personal and career development, helping shape my perspective on the overarching role of scientific research, development, and deployment in sustainability. Her honesty, practicality, flexibility, and positivity are traits that I hope to emulate in myself going forward.

I am also very grateful for my collaborators in the Plata Lab on the methane abatement catalysis project, including Audrey Parker and Rebecca Brenneis, as well as the research and teaching staff in the Department of Materials Science and Engineering who have generously helped me on this project, including Geetha Berera, Charlie Settens, and Shaymus Hudson, and in the Department of Chemical Engineering, Taehoon Lee.

I would also like to thank my friends, especially Jack Gurev and Ixa Gani, and my partner, Span Spanbauer. Lastly, I would also like to thank my parents, Blythe and Joe Wilkinson, for their unconditional love, respect, and support as I have worked to chart my own path.

Contents

Introduction

Methane is a powerful and threatening greenhouse gas with a 20-year global warming potential 84 times that of carbon dioxide [1]. Its emissions represent 20% of global yearly greenhouse gas emissions by tonnage, making it second in both climate forcing and prevalence only to carbon dioxide [2], and an approximately equal climate forcing agent when considered under decadal timescales. Despite its extensive and rapidly increasing emissions, which have caused the global methane levels to increase by a factor of 2.6 since pre-industrial conditions [3], its overall atmospheric concentration is low: it has an average ambient concentration of less than 2000 parts per billion and a threshold level of 3.5-4% (the concentration at which the air becomes flammable; such elevated concentrations are extremely dangerous). Beneath this threshold level, elevated methane levels can range from 0.5%-2%, achievable in some industrial conditions (e.g. dairy barns and coal mines). Outside of these industrial conditions, methane emissions sources are diffuse and varied. Natural and biological sources are responsible for approximately half of all methane emissions.

Methane is classified as a short-lived climate pollutant: its atmospheric lifetime is 12 years [3]. Chemical processes in the atmosphere convert methane to carbon dioxide, which has an estimated atmospheric lifetime of 300-1000 years; in contrast to atmospheric methane conversion, the primary avenue for atmospheric carbon dioxide conversion is for it to *exit* the atmosphere entirely via geologic and biologic processes including rock weathering, ocean uptake, and plant/microbial photosynthesis.

Given methane's high initial warming and its eventual atmospheric fate, it follows that a promising strategy for short-term climate mitigation would be to accelerate the timeline for methane conversion into carbon dioxide, preventing the immediate climate forcing caused by methane while having relatively little effect on the overall emissions of carbon dioxide [4]. Recognizing this, methane abatement catalysis is a new and growing field. However, deployability of initial research in the field has been limited due to the temperature and atmospheric composition requirements of most catalysts, as well as generally low reaction rates and percent conversions achieved so far [5, 6]. As more than 350 million tonnes of methane are emitted each year [7], it is of paramount importance that developed solutions be high-throughput, economical, and scalable in order to have the potential to impact global climate change.

The Plata Lab at MIT has recently developed a highly-promising methane oxidation catalyst that achieves complete conversion at 300-400 °C and oxygenic atmospheric conditions [8]. The catalyst, composed of copper-doped mordenite (a class of zeolite), is notable for its earth-abundance, cost-effectiveness, and efficiency at low concentrations, the latter achieved via inspiration from methane monooxygenase enzymes seen in methanotropic bacteria [9, 10].

Initial testing of the catalyst has proved efficacy for up to 300 hours [8] of continuous performance; however, longer-term performance has yet to be established. Materials characterization and spectroscopy experiments were chosen to investigate the stability of the catalyst over time, specifically with respect to elevated temperatures that the catalyst would experience in deployment settings. The primary two properties considered likely to degrade over time were surface area (and therefore number of available active sites) and structure/phase integrity. Therefore, the following techniques were chosen: scanning electron microscopy (SEM), to image the catalyst surface, in tandem with electron dispersive X-ray spectroscopy, to quantify and map the spatial element distribution; Brunauer–Emmett–Teller Analysis (BET), to model the effective surface area of the catalyst quantitatively; differential scanning calorimetry (DSC), to identify phase transitions that appear upon heat cycling and to

calculate temperature-dependent heat capacity; and, lastly, X-ray diffraction (XRD), to generate spectra that identify and quantify the presence of different phases in the material.

In this thesis, we describe the methodology used to characterize the evolution of catalyst samples, processed at 400 °C and 950 °C for extended periods of time, and report results showing that the catalyst is stable for long-term operation at 400 °C, but degrades through sintering and phase transition after a short time at 950 °C. This indicates viability for long-term operation at 400 °C reaction conditions with a need for a reactor controls strategy to manage occasional high-methane bursts that may result in elevated temperatures.

Methods

Copper-zeolite catalyst samples were synthesized following the methods previously published in [8].

1. Combine 9.3 g Acros Organics copper (II) nitrate trihydrate and 7.5 g Thermo Scientific zeolite mordenite, ammonium with 750 mL Milli-Q ultrapure water.

2. Mechanically agitate mixture for six hours on shaker apparatus.

3. Vacuum-dry mixture through glass fiber filter paper onto petri dish.

4. Dry filtered solids at 130 °C in Thermolyne muffle furnace for 12 hours.

This process was repeated as necessary to create the required mass of catalyst for the set of experiments. Syntheses were conducted in parallel, with 8 samples undergoing each step at a time. A total of 24 samples were synthesized and mixed before being placed into 16 beakers. These 16 beakers were then split into two groups in two Thermolyne benchtop muffle furnaces, held at 400 °C and 950 °C, respectively. Each beaker represented a sample that was to be taken out at a specific time: 3 days, 7 days, 14 days, 1 month, 2 months, and 3 months. Two backup beakers were reserved for replicate or replacement data but were not used. Control samples were also generated following the same synthesis and 130 °C drying procedure; rather than being placed into a beaker in the furnace, however, these samples were reserved and stored in a desiccator until testing. After being removed from the furnace at the designated

time, each sample was removed from the beaker, weighed into a glass vial, and stored in a desiccator until each characterization experiment was performed. Samples were allowed to air-cool and always rested a minimum of 1 day before each characterization experiment; all characterization experiments were conducted symmetrically such that every time-pair of data points (for example, the pair of 7 day samples that were held at 400 °C and 950 °C each) was stored for the same amount of time and tested on the same day. Each characterization method was conducted in the same way for every measurement, described individually for each technique below. With the exception of DSC heat cycling, all tests were conducted at room temperature.

2.1 Analytical techniques

2.1.1 Scanning Electron Microscopy - Electron Dispersive X-Ray Spectroscopy (SEM-EDS)

SEM imagery was taken on a Zeiss Merlin high resolution SEM with an EDAX EDS attachment. The SEM images were all taken at 15,000X magnification under Analytical mode with a working distance of 6-6.1 mm. The EDS images were all taken at 7,500X magnification with a working distance of 14.8-14.9 mm, with the exception of Sample A, which was taken at 20.4 mm working distance. SEM imagery was visually evaluated for changes in surface characteristics. EDS imagery was processed through the EDAX APEX software to produce elemental maps, summary spectra, and tables detailing samples' elemental compositions.

2.1.2 Brunauer–Emmett–Teller Analysis (BET)

BET analyses were conducted on a Micromeritics 3Flex instrument, with capacity for simultaneous analysis of 3 samples at a time. Samples were degassed prior to each analysis at 130 °C. Adsorptive analysis was conducted under N2 gas at 77.440 K until the sample had saturated with gas, approximately 5 days per set of samples.

It should be noted that BET analysis relies in part on prior modeling assumptions and is more of a "model" than a "measurement" [11]. There are also standing questions and scientific discourse about the accuracy of BET analysis for materials such as mordenite zeolite with particularly small pore sizes less than 7 Å[12]. Therefore, one should not take the results of this BET analysis to be a highly accurate quantitative measurement of true physical pore size, volume, and surface area. Our results do show extreme changes in these quantities, and our BET analysis can be considered strong evidence of these relative changes.

2.1.3 Differential Scanning Calorimetry (DSC)

DSC measurements were taken on a TA Instruments Q-Series DSC using aluminum T-Zero pans. In order to calculate heat capacity, two reference scans were taken at the beginning of every measurement session: a "baseline" scan with only empty pans inside the chamber, and a "standard" scan containing a sapphire sample with a known heat capacity. Heat capacities were then calculated using the following formula:

$$C_c = \frac{C_s h_c m_s}{h_s m_c}$$

where C_c and C_s are the heat capacities of the catalyst sample and the sapphire standard respectively, m_c and m_s are the masses of the catalyst sample and sapphire standard respectively, and h_c and h_s are the heating rates of the catalyst sample and the sapphire reference respectively.

Each heat capacity was calculated as a function of temperature from 20-400 °C (the maximum temperature of the instrument). It was noted that the first cycle from 20-400 °C contained multiple peaks in its DSC curves, likely resulting from bound water/gas releasing when heated; thus, each sample was run for 3, 20-400 °C cycles in the DSC and only the third cycle was used for heat capacity calculations. The results of the first cycle are also presented in the Results section along with a likely interpretation. As data taken near the beginning of each cycle was often inconsistent

due to machine equilibration, data was only used for calculation, and heat capacities are only reported, in the range 50-400 °C.

When presenting the first cycle heat flows and third cycle heat capacities, each data point was normalized before graphing. For the heat flows, each measured heat flow was divided by the initial (pre-cycle) sample mass. For the heat capacities, we assume that the average heat capacity in the range 50-400 °C is 1.28 as obtained in [13], since the absolute heat capacity of the sample was indeterminable due to an unknown, unmeasured quantity of bound water originally present in the sample.

2.1.4 X-Ray Diffraction (XRD)

XRD spectra were taken with a PANalytical X'Pert Pro using a Cu target and a high-speed, high-resolution X'Celerator detector from 10-90 2θ with a 15 min scan time. These spectra were compiled and analyzed with the HighScore Plus XRD analysis software for peak-fitting, structure-matching, phase identification, and phase quantification. Potential phase candidates were chosen by referencing the phase diagram for silicon dioxide and searching within the HighScore Plus phase database. Trends were assessed visually, though in future work it would be possible to take a more quantitative approach to assessing e.g. amorphous vs. crystalline composition or changes in lattice parameter over time. Phase identification was performed on the control sample, the first 400 °C sample, and all 950 °C samples. Phase identification in HighScore Plus relies on initial assumptions about what phases are likely to be present in the material and is limited by its database. Phase quantification is calculated from the phases that are found during the identification step.

Results

This chapter describes the results from the four experiments performed on the copper-zeolite methane oxidation catalyst. Analyses were performed on samples held at 400 °C or 950 °C over 3 days, 7 days, 14 days, 1 month, 2 months, and 3 months, and control samples.

Section 3.1 contains Scanning Electron Microscopy (SEM) images of the catalyst depicting sintering of the catalyst samples held at 950 °C. It also gives the elemental composition of the sample's surface obtained via Electron Dispersive X-Ray Spectroscopy (EDS), showing no significant change among the samples besides possible formation of potassium and calcium deposits on the surface of the 950 °C samples.

Section 3.2 presents a Brunauer-Emmett-Teller (BET) analysis of the samples, showing that the samples held at 950 °C exhibit a dramatic decrease in pore size and surface area within three days.

Section 3.3 provides Differential Scanning Calorimetry (DSC) of the samples showing outgassing over the first heating cycle followed by consistent measurements of the heat capacity over subsequent cycles.

Section 3.4 gives X-Ray Diffraction (XRD) spectra of the samples showing stable crystal structure for the 400 °C samples and a progressive phase transition to a mixture of mullite, cristobalite, and quartz in the 950 °C samples.

3.1 SEM-EDS

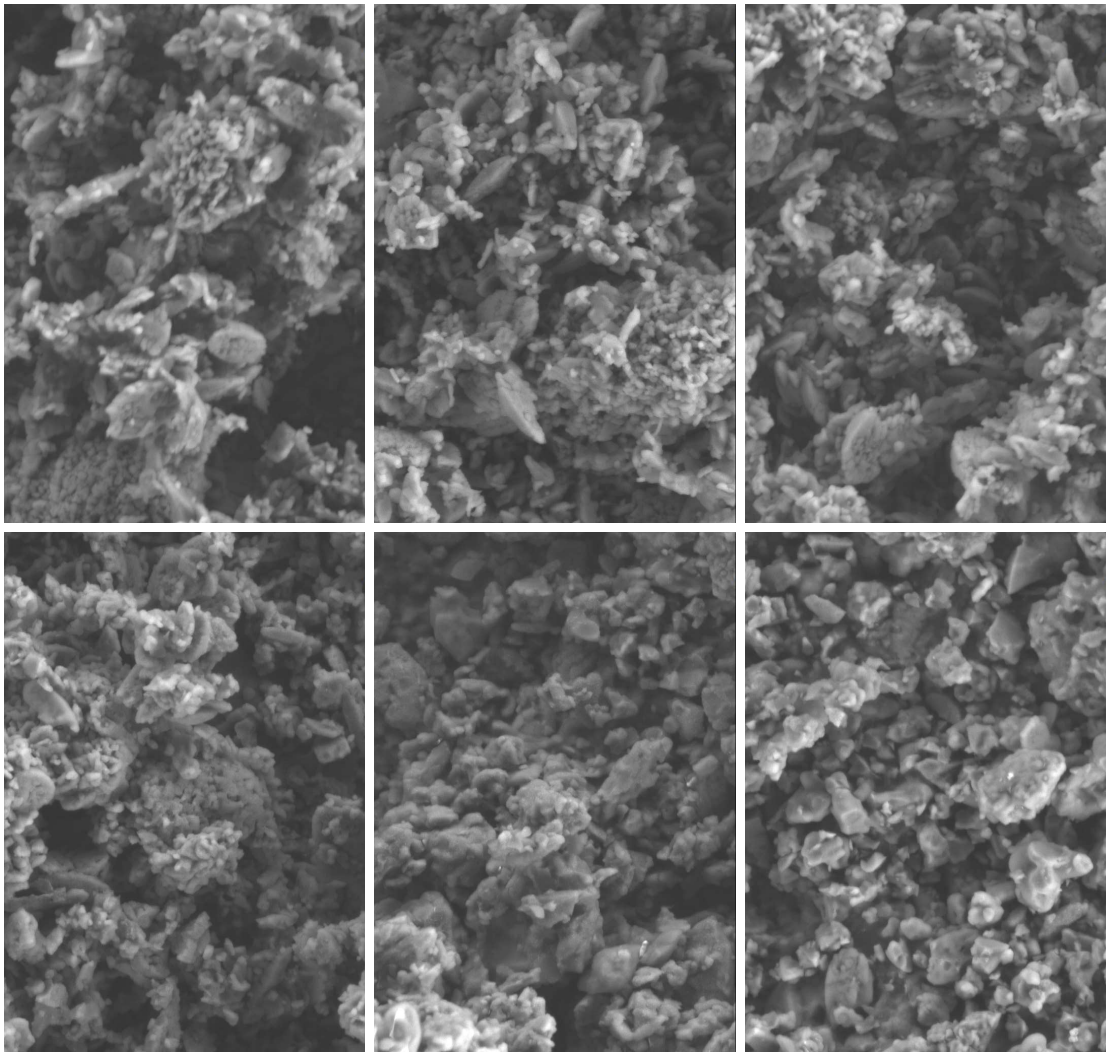

Figure 3-1: SEM images at 15000X magnification. 400 °C samples at 3, 7, and 14 days are listed in the top row, and 950 °C samples at 3, 7, and 14 days are listed in the bottom row. The 400 °C samples show a rough, porous surface that appears to sinter and become more smooth over time in the 950 °C samples.

The SEM images shown in Figure 3-1, captured at 15,000X magnification, depict powdered catalyst placed on conductive tape. The purpose of these images was to produce a visual reference for microstructure surface area (not catalytic surface area) and roughness. It is shown that the 400 °C samples have a high surface area with significant pitting and texturing. These sample images do not appear to have

substantial features, nor do they show apparent changes over time. They appear to simply reflect the original grinding and powdering process used to produce the catalyst and adhere it to the sample holder. Thus, we conclude that the 400 °C samples are exhibiting no surface changes, and in particular that they are not sintering.

The 950 °C samples show a different behavior than the 400 °C samples. While the initial 3-day sample appears highly textured, the 7-day and 14-day samples lose this resolution, showing larger, smoother structures. This indicates that the material is sintering, a conclusion that is corroborated with the BET data.

Element	**A**	**B**	**C**	**D**	**E**	**F**	**I**	**J**	**K**	**L**	**M**	**N**
O	52.6	56.8	52.0	56.7	55.2	53.3	52.3	60.8	55.1	45.1	53.8	52.9
Na	0.4	0.8	0.6	0.8	0.7	0.6	0.5	1.4	0.8	0.4	0.6	0.6
Al	5.0	4.1	4.5	4.0	4.2	4.4	4.0	4.2	4.7	4.2	4.3	4.4
Si	40.0	35.4	39.4	35.5	37.0	38.6	37.0	28.3	34.5	44.1	38.2	39.3
K	0.1	1.2	1.1	1.5	1.37	1.7	3.0	1.7	1.6	3.5	1.6	1.4
Ca	0.1	0.0	0.2	0.0	0.0	0.0	1.5	2.5	1.7	0.0	0.2	0.1
Cu	1.8	1.7	2.3	1.7	1.49	1.5	1.7	1.1	1.6	2.7	1.5	1.4

Table 3.1: Proportion (%) of element on surface by weight obtained by EDS

EDS measurements of the elemental composition of each sample's surface is shown in Table 3.1. The surface composition appears largely stable over time, for both the 400 °C and the 950 °C samples. Notably the surface concentration of copper was found to be 1.1-2.7% regardless of which temperature the sample was held at, which is within the variability of the synthesis and measurement methods. This demonstrates that the catalyst is not degrading due to loss of copper, which was a previous concern about long-term operation. Furthermore, the elemental maps of both the 400 °C and the 950 °C samples, not depicted, were well-mixed, mitigating concerns that the degradation in the 950 °C samples was due to agglomeration of copper. It does appear that deposits of calcium, and to a lesser extent potassium, formed on the surface of the 950 °C sample for samples I, J, and K, likely through migration.

3.2 BET

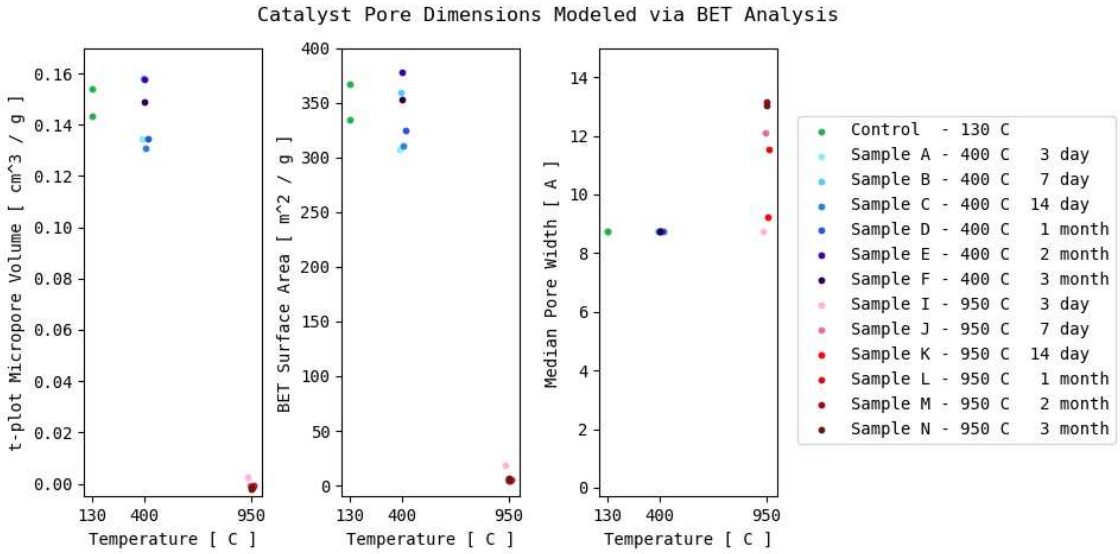

Figure 3-2: Summary of properties estimated by BET analysis for each sample, left-to-right: t-plot micropore volume, BET surface area, and median pore width.

From the t-plot micropore volume and BET surface area shown in Figure 3-2 it is evident that the surface properties of the 950 °C samples are strongly affected by their heat treatment. The 400 °C samples exhibit high surface areas of >300 m^2/g, comparable to the control 130 °C sample, while the 950 °C samples have low surface areas of <20 m^2/g. Common interpretation of these values classify the 400 °C samples as "highly porous" and the 950 °C samples as "practically nonporous", indicating significant transformation has occurred in the 950 °C samples that would render the catalyst nonfunctional. Calculated median pore width is consistent between the control and 400 °C samples but highly variable with the 950 °C samples, which is consistent with the limitations of estimating pore width of a nonporous material. Heat treatment effects characterized by BET are seen immediately, with minimal evolution over time in either temperature category. The highest BET surface area is seen in the 400 °C 2 month sample.

3.3 DSC

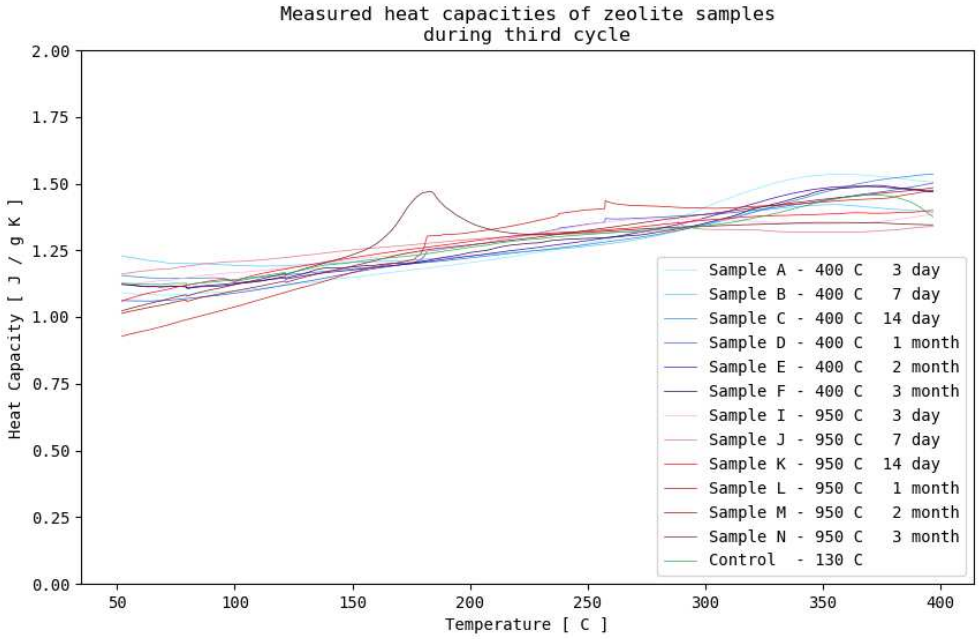

Figure 3-3: Computed heat capacity (normalized to match reference data) of each sample in the range 20-400 °C as calculated from DSC data. The third heat cycle quantifies the heat capacity of the catalyst itself, removing the effect of adsorbed water-gas loss peaks which appear in the first cycle as can be seen in Figure 3-4.

DSC was performed to assess thermal stability to repeated heat cycling in the range 20-400 °C. Each sample was heat cycled three times. Heat capacities were calculated from these experiments on the third cycle, found in Figure 3-3. Heat capacities ranged from 0.9-1.5 $\frac{J}{gK}$ over the course of all heat cycles, increasing with temperature. There was not a significant difference in trend between 400 °C and 950 °C samples, but there was significant sample-to-sample variability; this was likely a result of the unknown, unmeasured difference in initial water content between samples, as well as instrument limitations.

These values approximately correspond to empirical results reported in literature at low temperatures, albeit with significant experimental variability, which is also seen in the published literature [14, 15]. There is a pronounced difference in litera-

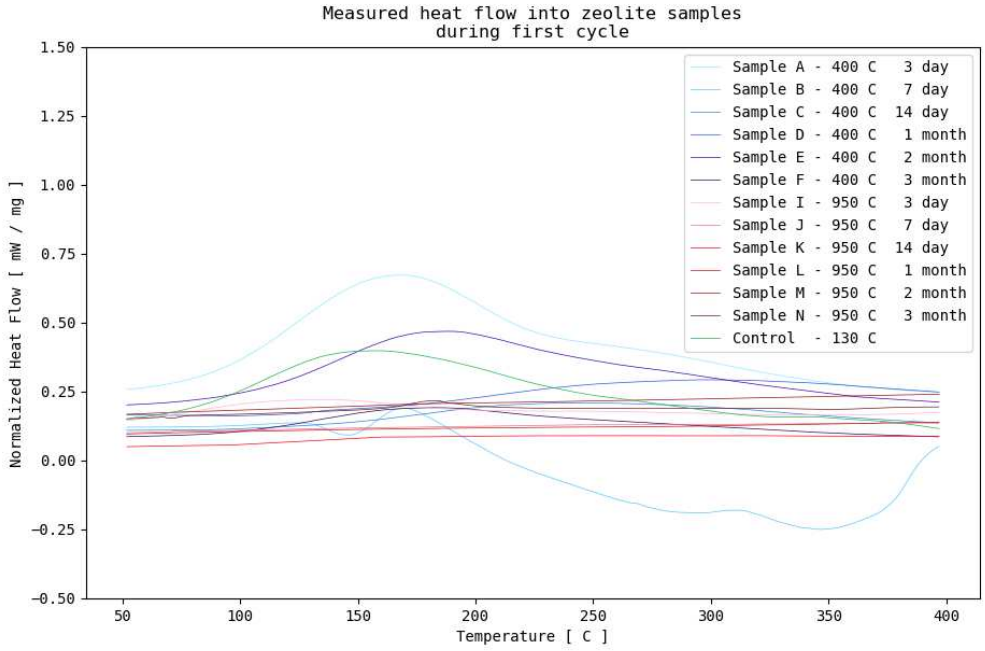

Figure 3-4: Measured heat flow (normalized by initial sample mass) through each sample as measured by DSC. Note the differing water-gas loss peaks appearing in the control and 400 °C samples. Existing literature on mordenite zeolites [16] offers one strong explanation: loss of water accompanied by release of ammonia up to 260-360 °C, followed by dehydroxylation at higher temperatures.

ture between heat capacities measured experimentally and heat capacities estimated from thermodynamic calculations, the former being generally higher than the latter [13].

Peaks in heat flow indicate the presence of phase transitions, though they do not identify them chemically. Samples, particularly 400 °C samples, seem have multiple peaks during their first heating cycle (as seen in Figure 3-4), indicating presence of multiple transitions per sample. As each sample was structurally identified via XRD and elementally via EDS, it seems most likely that these transitions represent the lifting of various adsorbents from each material, acquired during or after the heat treatment process. Supporting this, phase transitions between 127-360 °C have been found in literature to be bound water and release of ammonia; higher temperature transitions most likely correspond to water release via dehydroxylation [14, 16].

The 950 °C samples appear to have less variable, and weaker, phase transitions observable in initial heat cycles. This is consistent with the reduced surface area available to adsorbents in those 950 °C samples demonstrated by BET analysis (Figure 3-2).

3.4 XRD

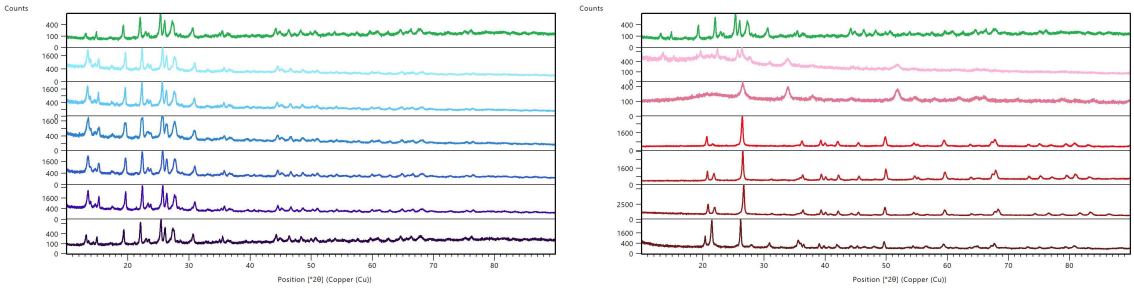

Figure 3-5: Measured XRD spectra for all samples from 10-90 degrees 2θ. The control sample is shown in green. 400 °C scans are shown in the left pane with cool colors (A, B, C, D, E, F from top to bottom); 950 °C scans are shown in the right pane with warm colors (I, J, K, L, M, N from top to bottom).

XRD was performed to show the evolution of crystal structure and phase identity over time. The blue samples shown in Figure 3-5, heat treated at 400 °C, show a constant pattern identified as mordenite zeolite. The red samples, heat treated at 950 °C, show a peak-broadening effect from the 400 °C pattern starting at 3 days, that the 7 day pattern seems to continue; this is generally indicative of higher amorphous content likely to occur during phase transition. In the 14 day and beyond patterns, new, sharp peaks begin to emerge, indicating that the phase transition is completing, and the sample is settling into a new crystalline phase mixture.

Each phase identification is presented individually in Figure 6-1. Every 400 °C sample was identified as remaining mordenite zeolite, whereas samples held at 950 °C for at least 14 days were identified as a phase mixture of mullite, cristobalite, and quartz. The samples held at 950 °C for less than 14 days appear to be in transition from mordenite zeolite to this new phase mixture.

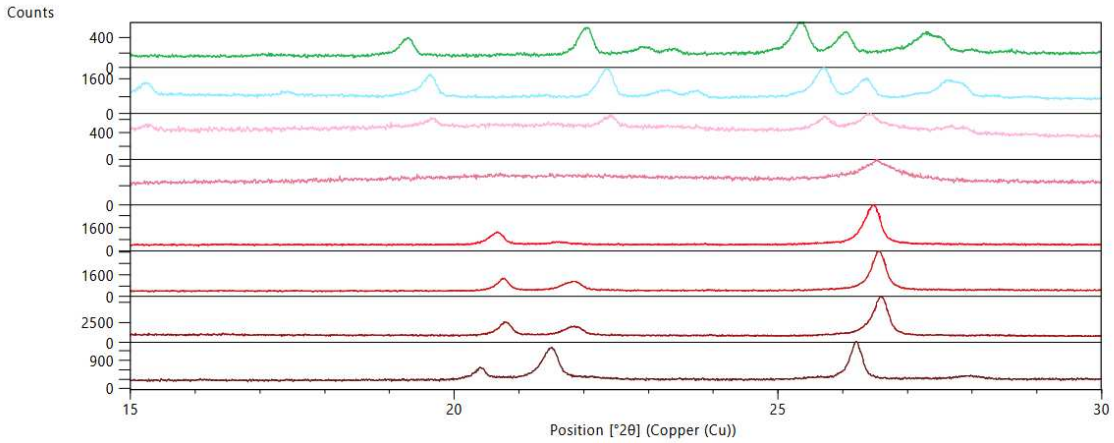

Figure 3-6: A zoomed-in comparison of the control sample and samples A, I, J, K, L, M, and N, showing the gradual transformation that the 950 °C samples undergo. Samples I and J still resemble the original mordenite phase pattern, but seem to exhibit significantly more amorphous character, potentially as an intermediate state during a phase transformation. Samples K, L, M, and N show a strong, crystalline, altogether different diffraction pattern.

Discussion

Copper-exchanged zeolite catalysts have a long history [17] and a well-understood exchange mechanism; they have seen extensive commercial deployment in the automotive industry for engine exhaust filtration [18, 19] for nitrogen monoxide removal [20, 21, 22], as well as application in oil refining [23].

Before its utility in climate change mitigation became apparent, copper-exchanged zeolites were also used for the partial catalytic oxidation of methane to methanol using natural gas sources [24, 25, 26]. This application is actually more technically complex than our use-case: conversion of methane to methanol requires achieving selective partial oxidization of the methane, whereas we simply aim to fully oxidize the methane. Thus our research is not unprecedented in concept, but instead aims to leverage a fairly well understood class of catalysts towards a timely problem that they are very well-suited to solve. The primary challenge lies in rapidly optimizing the catalyst for methane removal, and demonstrating technical readiness through rigorous materials testing in increasingly realistic settings, leading up to field testing and deployment.

The four studies were chosen to, when analyzed collectively and in conversation, provide a comprehensive understanding of the stability of the catalyst under extended heat treatment. The primary goal was to understand the presence and content of active sites and the materials structure over time.

The 400 °C samples showed similar behavior throughout the four experiments and over time. SEM visuals were as expected with rough, porous surfaces that lacked distinction; this was supported by EDS spectra showing well-mixed distribution of copper in the catalyst, and BET data showing high calculated surface area. XRD showed consistent structure thoughout, identified as the mordenite phase as previously expected. DSC heat cycling produced phase transitions that were identified in the literature as water loss; zeolites contain bound water that is stripped along with ammonia in range of 20-400 °C [14, 16]. However, this water is not associated with the methane oxidation reaction and these phase transitions were not seen in the second and third cycles of each DSC run, implying that these phase transitions would not occur continuously under operation conditions and would not significantly or permanently affect catalyst structure/integrity. While experimental repetition to achieve statistical significance was not undertaken, all 400 °C sample data were qualitatively and approximately-quantitatively consistent with control sample data.

The 950 °C samples underwent a slow, complex transformation as seen by multiple experimental methods. These transformations, beginning in as few as three days but extending throughout the three-month experimental period, result in progressive catalyst degradation leading to full deactivation. The four experimental methods chosen show different rates of catalyst transformation. While the 3 day BET analysis shows strong and immediate decrease in catalytic surface area, which is supported by the lack of bound/adsorbed phase transition peaks seen in 3 day DSC, SEM imagery does not show visually apparent micron-level sintering until 14 days, the same timepoint at which XRD phase analysis exhibits complete disappearance of the mordenite phase in the material.

This may be explained by the differing scale of each measurement process: BET yields information about the smallest spatial scales of the analyses we conducted, as it is used for Angstrom-level catalytic surface area and pore dimension calculations, whereas SEM images are on the micron-scale and XRD spectra represent microstructural but bulk phase properties. As it is logical that changes in the structure of the material

go from "small to large", this difference in time-scales is not unexpected.

The smallest-scale experimental method, BET, clearly shows a dramatic transformation of the material in just three days of high temperature operation, with pore volume and surface area dropping very significantly, and pore width behaving variably but generally increasing. (Variability in estimated pore width may also reflect that the eventual phase mixture does not have pores.) The other three analyses demonstrate similar, but slower, larger-scale changes, not only in surface area decrease, but also in sintering and phase transition to a mixture of mullite, cristobalite, and quartz.

While future work in the 1-3 day period may confer more information about the "order of operations" in catalyst transformation, particularly if in-situ observations were undergone to understand the mechanisms of this progression (i.e. proportion and progression of sintering vs. phase transformation) remain of scientific curiosity, it is evident from an engineering standpoint that 950 °C conditions are detrimental to the catalyst and should be avoided as a matter of catalyst optimization.

4.1 Catalyst Optimization

Catalyst optimization, and particularly prevention of catalyst degradation and deactivation, is a rich area of study due to its pervasive use throughout industry; catalyst integrity is a prerequisite for operation of many of the reactions that power modern human life, including in the production of fertilizer via Haber-Bosch and the production of fuels via catalytic cracking. It is also a complex and often highly empirical area of study due to the wide variety of processes that can degrade catalysts, including surface- or structural-level mechanical degradation, poisoning, leaching, fouling, or coking [27]. The predominant method of catalyst degradation tested and observed in this work was sintering and phase transition.

Sintering at high temperatures appears to be an irreducible constraint of this catalyst and reaction; when kept at elevated temperatures for extended periods of time, the

catalyst will undergo deactivating phase transitions that persist even when the catalyst is brought back down to ambient temperatures. However, this constraint may be compensated for with a reactor controls system that prevents the catalyst from reaching elevated temperatures.

Zeolite catalysts can be poisoned by multiple different chemical species. Ammonia is a documented zeolite poison [28] present in dairy barns, which has fortunately been shown to be thermally reversible [29]; this is related to the observation in Figure 3-4 that water and ammonia are outgassed as the zeolite is heat cycled via DSC. Sulfur and metals (particularly Ni, Na, V, and Fe) are also known zeolite poisons [28]. Sulfur, which can appear in coal in concentrations upwards of 3% [30], has been shown to be an issue at low temperatures $<$250 °C but fortunately does not cause catalyst degradation above 300 °C [31]. Metal poisoning is a common problem seen in catalytic cracking of oil, and is generally handled by passivating these metals with additives such as bismuth or manganese [32]. It is unclear whether these metals are present or of concern in coal mine application.

Various catalysts, including zeolites, can be regenerated from poisoning through inert gas, air, or hydrogen purging at elevated temperatures, generally at conditions greater than 500 °C [33, 34, 35]. If our catalyst is found to be poisoned by contaminants present in industrial environments, purging at elevated temperatures (even at those which, long-term, cause sintering and phase transition) for short periods of time may recover catalyst efficiency. Analogous behavior was seen in previous work with our catalyst, with activation at 550 °C promoting temporarily high conversion efficiency at lower reaction temperatures, although this conversion efficiency decreased over time unless steady-state reactor temperature was 310 °C or greater [8]. This suggests periodic temperature elevation, or "re-activation" of the catalyst, is an avenue to be explored under circumstances of catalyst poisoning.

Zeolite catalysts are also known to undergo coking, a matter of particular concern in coal mine but not dairy barn applications. Deactivation results both from direct

poisoning of individual active sites by coke deposits and pore blockage that prevents transmission to multiple active sites [36]. Due to its narrow pore channels (through which it is more difficult for coke to diffuse and cause blockage than for larger-pore zeolites), mordenite is less susceptible to coking than other zeolites, but it is still susceptible [28]. While poisoning of individual sites may potentially addressed by re-activation, accumulation and blockage present physical challenges that are more easily prevented than repaired. Traditional industrial solutions to coking involve various filtration, purification, and separations processes, utilized extensively in oil refineries due to their need to maintain selectivity and produce valuable, differentiated petrochemical products [37]. While active separations techniques add technical complexity and energy costs, membrane-based filtration approaches are being considered for the reactor system and are a subject of ongoing research.

4.2 Reactor Optimization

In our experimental results and previous sections, we have found that it is critical to catalyst performance to maintain appropriate operation temperature. A future research and deployment question follows, then: how might this ideal operation temperature be maintained, and what energy burden does it impose?

By virtue of our reactor oxidizing the methane in the input gas, the reactor can be entirely self-heating (i.e. not require external heat except during startup) for a fairly wide range of methane concentrations. At very high concentrations of methane, some precaution may be required to avoid the reactor overheating (most simply diluting the input gas stream with plain air).

In this section, we compute estimates of the reactor steady-state operating temperature as a function of methane concentration, under the assumptions that:

- the input gas stream arrives at a temperature of 20 °C;
- the input gas stream has the same general composition as air (i.e. ∼79% nitro-

gen, ∼21% oxygen) before adding methane;

- the reactor is perfectly efficient and achieves complete conversion at oxidation;
- and the majority of heat generated in the reactor goes towards warming the input gas stream to the reactor operating temperature.

The last condition is roughly satisfied if the reactor is well insulated and the flow rate of the input gas is relatively high.

Under these assumptions, we need simply consider the heat of combustion, Q, of methane ($890.4\frac{kJ}{mol}$) [38] and the heat capacity, C_p, of the gas mixture in the temperature range under consideration in order to obtain an approximate steady state operating temperature for the reactor. While the heat capacity of the gas mixture increases with temperature (Figure 6-2), strongly so in the case of methane, the changes in heat capacity for nitrogen and oxygen, the majority components in the gas mixture, were relatively low. As a conservative approximation that allotted for potential inefficiencies in heating, we used only the final-temperature, highest heat capacity as a constant in each $Q = mC_p\Delta T$ calculation.

Given these assumptions and reference heat capacities, we computed estimates of the reactor steady state operating temperature as a function of methane concentration (4-1). We found that the region between 1% and 2.5% methane corresponded to optimal, self-sustaining behavior: the heat of oxidation was sufficient to heat the reactor to complete-conversion rates without generating excess heat that resulted in undesirable temperature increases. For operation at 400 °C, 1.4% methane was found to be the optimal concentration.

These concentrations are potentially achievable in both dairy barns and coal mines. However, there is great uncertainty about the concentration of methane in industrial environments, and even if methane concentration reaches 1.4% with regularity, lack of consistency in methane flux may pose an issue, resulting in concentrations that are either too low or too high [39, 40]. Measured methane emissions from industry,

including dairy/agriculture and oil/gas, has been consistently found to be underestimated from point-source measurements, a matter of both climate concern and engineering difficulty in responding to the methane problem [41, 42, 43, 44, 45, 46]. In some cases, empirical results or events seem to defy logical or predicted sense: methane emissions from coal mines are increasing despite decreasing coal production [47], dairy barns have exploded from spontaneous methane ignition despite low concentrations reported in some studies [48], and both anthropogenic methane emissions and methane-induced warming have been found to be underestimated in the predominant IPCC climate projections [49, 50]. While these contradictions are a call to action for greater measurement standards and reporting integrity, we find it most important to mitigate rather than count emissions, and hope to design a reactor that is flexible to whatever concentrations that it happens to experience, and incorporate measurement-response capability as sensor capacity and contextual knowledge is developed.

In the spirit of designing for variable methane concentrations, we note that the reactor operation is stable towards increasing methane concentrations or temperatures, since it takes an increasing amount of energy to warm the input air to higher temperatures. At excessively high temperatures or concentrations, however, we have shown earlier that the catalyst degrades and becomes ineffective. Thus, in extreme cases or if lacking operational controls, the reactor would 'fail cold', in that the catalyst would become nonfunctional, the reactor would stop oxidizing methane, and the reactor would cool back down. This failure mode should be easily avoidable by diluting the input gas stream if methane concentrations are too high.

However, the reactor is unstable towards decreasing methane concentrations. If the input gas stream is interrupted, or if methane concentrations drop significantly, the reactor will drop below a critical operating temperature and the catalysis will become less efficient. As previously shown by [8], complete conversion is only self-sustaining above 310 °C, and at temperatures lower than 200 °C, conversion rates decrease rapidly, creating a positive feedback loop of decreasing conversion efficiency and de-

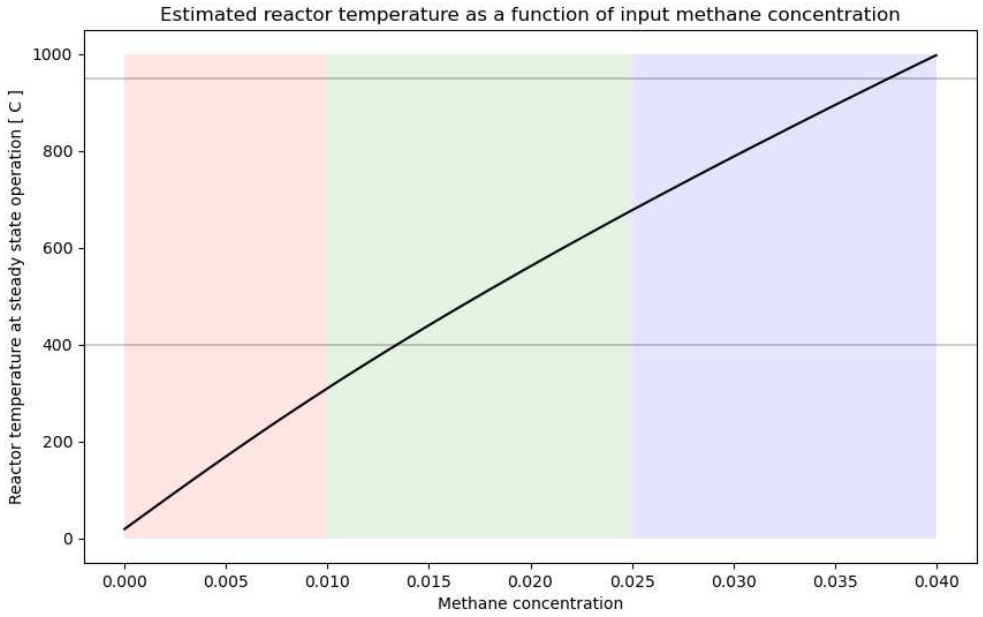

Figure 4-1: Steady-state operating temperature under the assumptions stated above. For methane concentrations below approximately 1% (red region) supplemental heating will be required to keep the reactor at a high enough temperature for efficient operation. For methane concentrations between roughly 1% to 2.5% (green region) the reactor will be able to maintain an appropriate operating temperature through oxidation of the methane in the input stream, avoiding the need for supplemental heating except during startup. For very high methane concentrations above roughly 2.5% (blue region) some care should be taken to avoid the reactor overheating. In this case, the simplest and most economical option is to dilute the input gas stream to a lower methane concentration.

creasing energy output to heat the reactor. Below a certain temperature, the reactor would essentially cease operation until actively heated back up. Although it presents a fixed energy cost, re-activation suggests a potential strategy to mitigate this effect, as brief excursions to high activation temperatures were shown to boost temporarily conversion efficiency at lower operation temperatures, thus creating an exit to the feedback loop that does not require continual energy input.

It is our conclusion that the reactor should be deployed with a control system which ensures that the reactor temperature never drops below a critical temperature. If the input gas stream has a relatively stable concentration of methane, and the reactor is designed with roughly this concentration in mind, then the reactor should be able to operate continuously without the need for additional energy input from the heating control system except during startup and to recover from disruptions. If periods of very high methane concentration are expected, the control system should additionally be capable of injecting additional plain air into the input stream to dilute the methane concentration and cool the reactor. If periods of very low methane concentration are expected, re-activation is a potential strategy to restore performance. Optimization of this reactor is the subject of ongoing research.

Conclusion

Methane has contributed an estimated .5 °C of global temperature increases since pre-industrial times [51], 2/3 the effect of carbon dioxide in the same period, and accounting for 1/3 of all warming due to greenhouse gases. Despite this, there is a significant lack of large-scale awareness and mitigation efforts dedicated to methane, particularly when compared to carbon dioxide. In 2023 the US Department of Energy invested $47 million in methane mitigation and removal, compared to $131 million in carbon dioxide mitigation and removal [52, 53]. It is a common climate misconception that carbon dioxide emissions are the sole climate-forcing agent of concern. However, methane emissions, with their faster and more severe impact relative to their extent, represent a perhaps more promising short-term target: it has been estimated that an emissions reduction of 45% by 2030 would prevent over .5 °C of warming by 2100 [54]. It follows that reducing the concentration of methane in the atmosphere, either by preventing emissions or by active removal, must then be a strong priority in global climate change mitigation efforts. Fortunately there has been a recent surge of research interest in methane mitigation, and significant progress has been made in finding economical, scalable solutions.

The Plata Lab at MIT reported a new zeolite-based methane removal catalyst [8] in 2021, capable of efficiently eliminating methane at concentrations commonly present in dairy barns and coal mines, two of the three leading sources of anthropogenic methane [55] (the other being emissions from oil and gas production, which, while at

concentrations appropriate for this catalyst, are more of an operations and maintenance problem). This thesis continues this new technology development, answering questions about the long-term stability and performance characteristics needed to accurately model the economics and climate impact of deploying this technology at scale.

We have demonstrated long-term viability of continual operation of the catalyst at moderate temperatures relevant to industrial methane removal. Specifically, we have shown the catalyst to be stable at 400 °C for three months, and have provided evidence that the catalyst has not undergone an observable level of degradation in those three months, strongly suggesting a much longer useful lifetime. We have also shown that the catalyst does degrade via sintering and phase transformation after as little as 3 days at 950 °C, thus establishing that the appropriate operating range for this catalyst is around 400 °C.

While our characterization regimen demonstrates catalyst stability at industrially relevant temperatures, it does not directly test performance in an industrial operational environment. Long-term performance characteristics while scrubbing high concentrations of methane in gas mixtures containing other pollutants or impurities are still uncertain. Future work involving field testing and techno-economic and life-cycle analyses will be required to answer these questions and firmly demonstrate economic/practical viability of at-scale deployment.

Given the importance of methane removal to our global climate change mitigation efforts and the existence of apparently viable methane removal catalysts such as the one studied here, the author is optimistic that an inexpensive, effective solution for industrial methane emissions could be deployed widely and rapidly once appropriate regulatory requirements and economic incentives are established.

Appendix

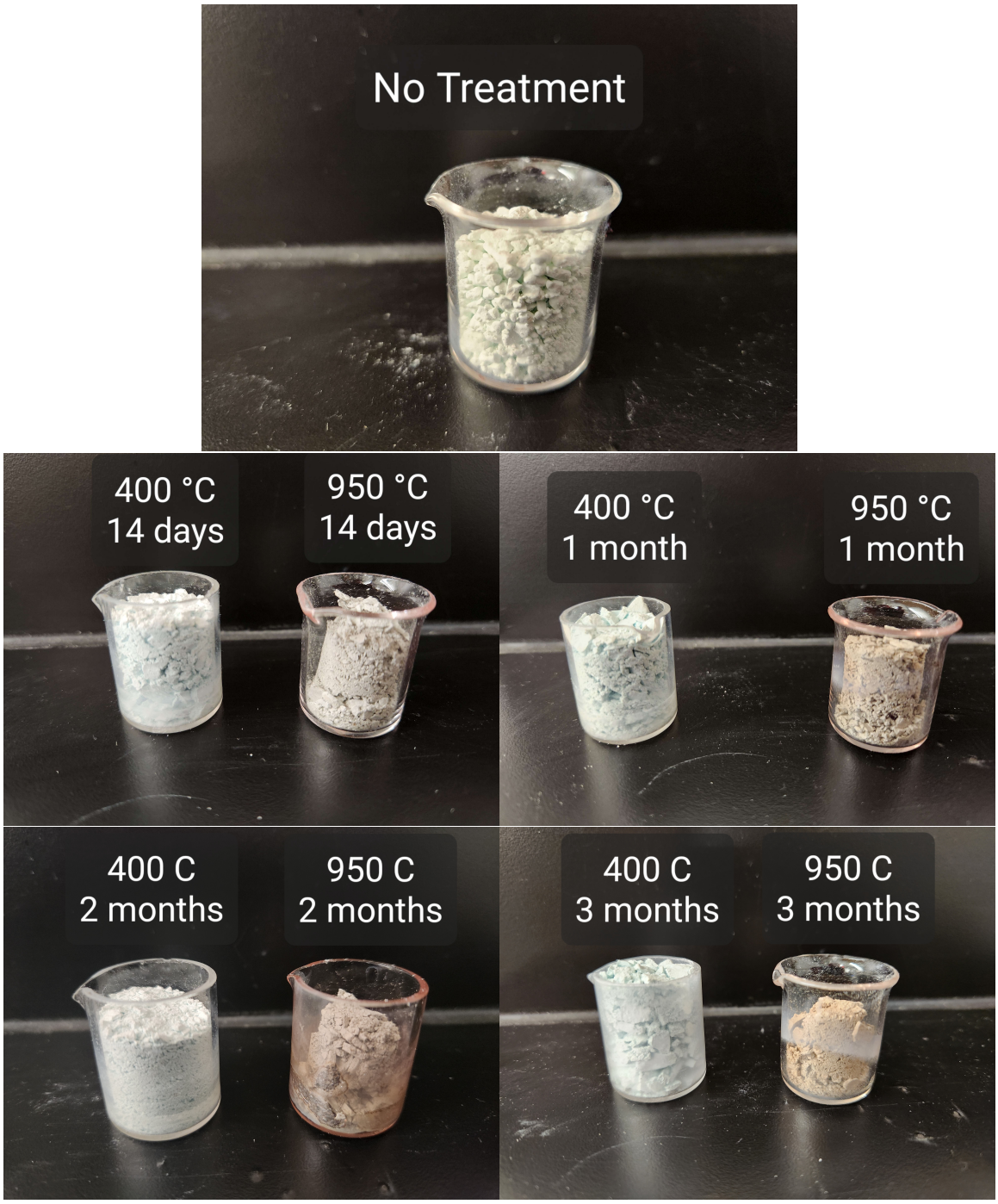

Figure 6-1: Pictures of samples after they were removed from the muffle furnace and before they were put into storage. 400 °C and 950 °C samples are easily visually distinguished from each other; 400 °C samples appear loosely-packed and with a blue-ish tinge, while 950 °C samples become densely-packed and brownish-grayish over time.

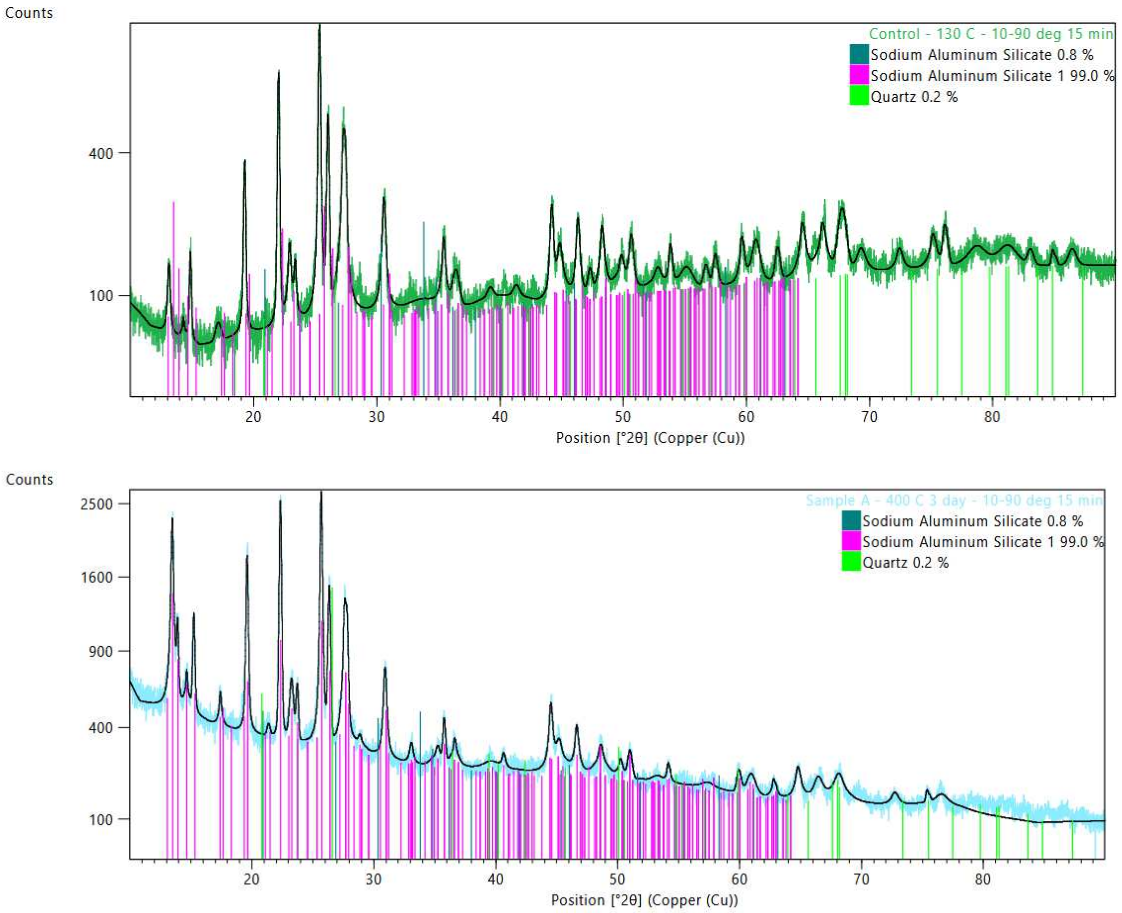
Counts
Control - 130 C - 10-90 deg 15 min
Sodium Aluminum Silicate 0.8 %
Sodium Aluminum Silicate 1 99.0 %
Quartz 0.2 %
400
100
20
30
40
50
60
70
80
Position [°2θ] (Copper (Cu))
Counts
Sample A - 400 C 3 day - 10-90 deg 15 min
Sodium Aluminum Silicate 0.8 %
Sodium Aluminum Silicate 1 99.0 %
Quartz 0.2 %
2500
1600
900
400
100
20
30
40
50
60
70
80
Position [°2θ] (Copper (Cu))

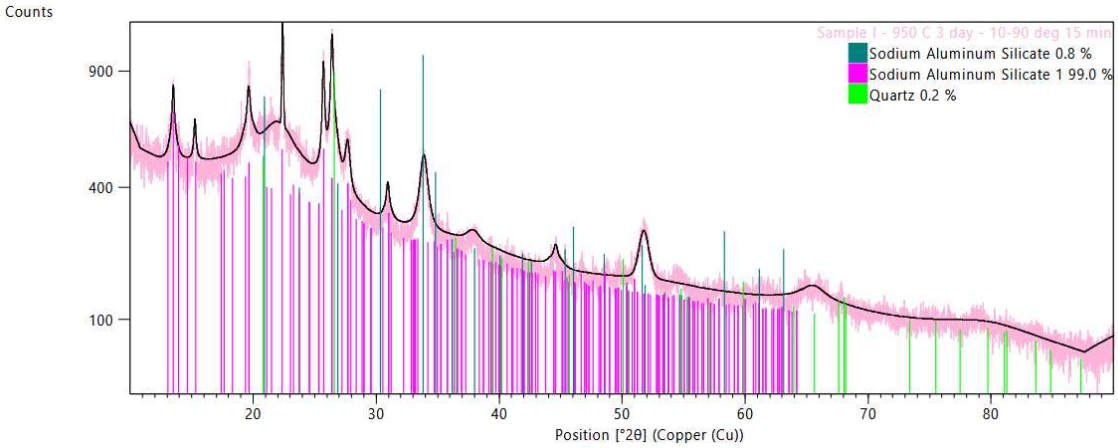
Counts
Sample I - 950 C 3 day - 10-90 deg 15 min
Sodium Aluminum Silicate 0.8 %
Sodium Aluminum Silicate 1 99.0 %
Quartz 0.2 %
900
400
100
20
30
40
50
60
70
80
Position [°2θ] (Copper (Cu))

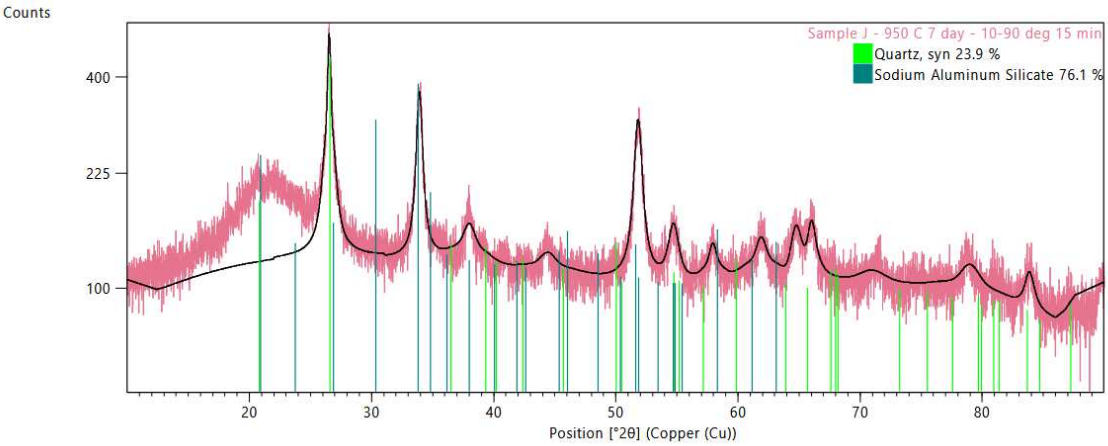
Counts
Sample J - 950 C 7 day - 10-90 deg 15 min
Quartz, syn 23.9 %
Sodium Aluminum Silicate 76.1 %
400
225
100
20
30
40
50
60
70
80
Position [°2θ] (Copper (Cu))

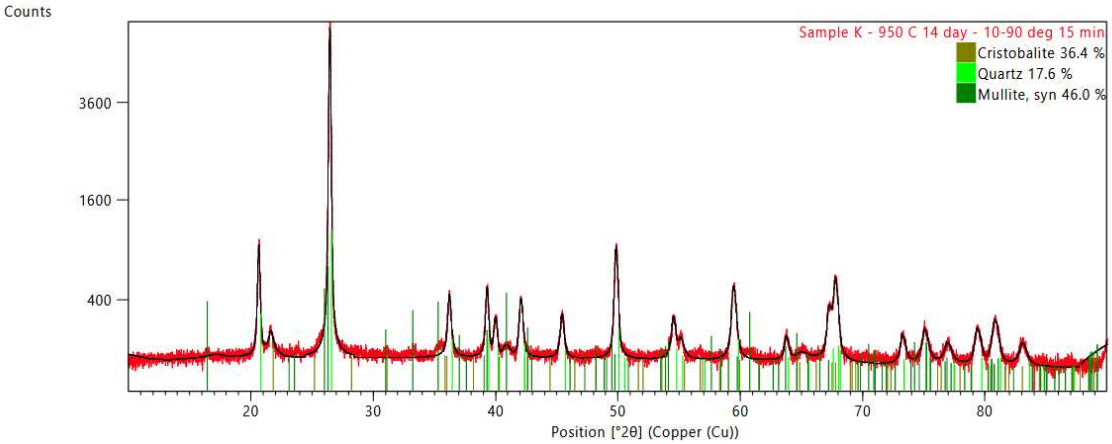
Counts
Sample K - 950 C 14 day - 10-90 deg 15 min
Cristobalite 36.4 %
Quartz 17.6 %
Mullite, syn 46.0 %
3600
1600
400
20
30
40
50
60
70
80
Position [°2θ] (Copper (Cu))

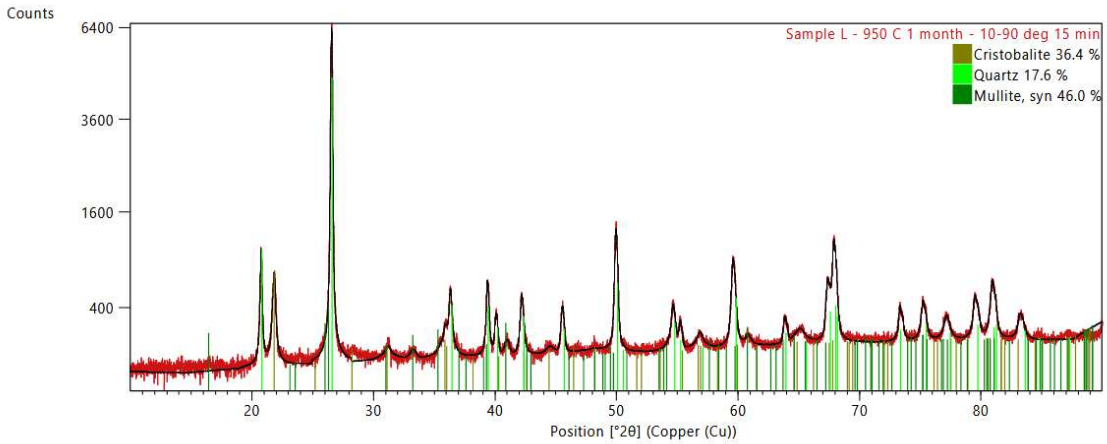
Counts
Sample L - 950 C 1 month - 10-90 deg 15 min
Cristobalite 36.4 %
Quartz 17.6 %
Mullite, syn 46.0 %
6400
3600
1600
400
20
30
40
50
60
70
80
Position [°2θ] (Copper (Cu))

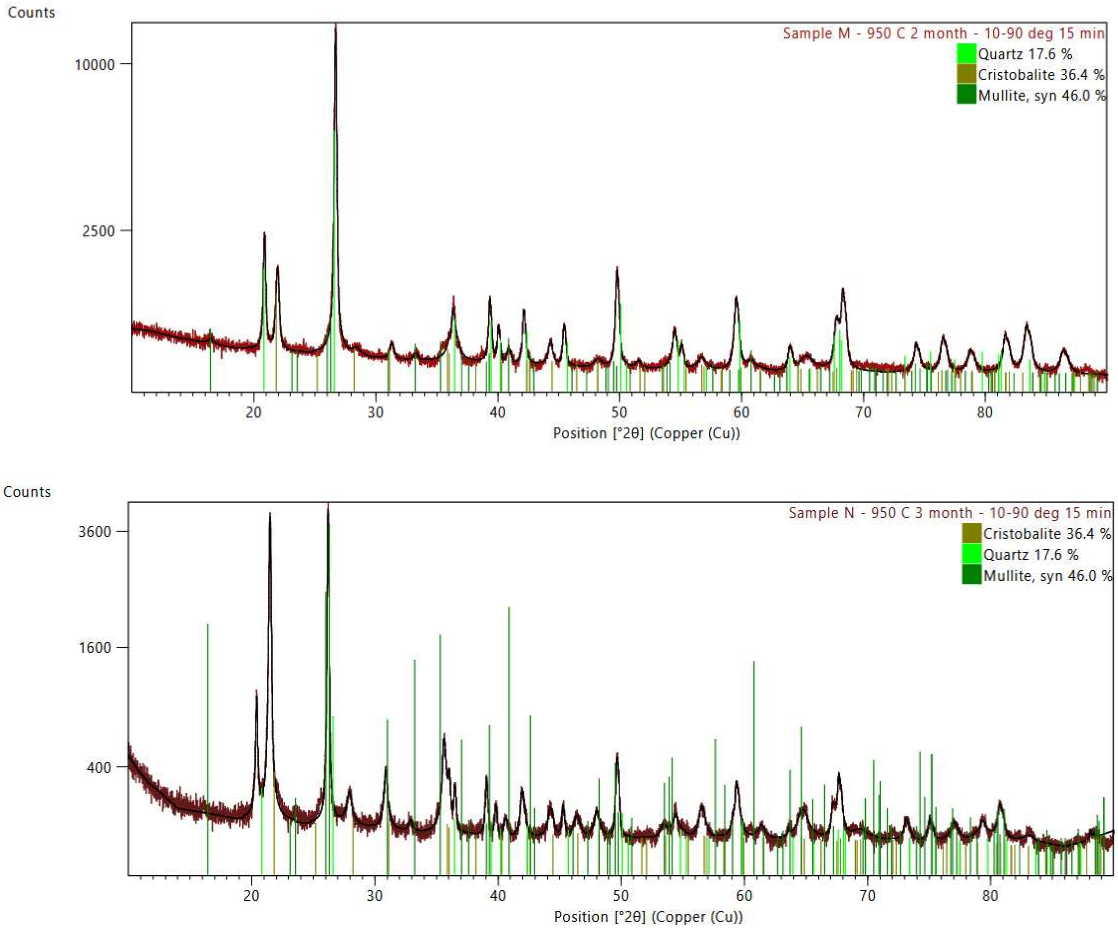

Figure 6-1: XRD phase identification of control sample and samples I, J, K, L, M, and N. Experimental spectra are shown overlayed with phase identification patterns in addition to their phase quantification data. The two Sodium Aluminum Silicate patterns are two different patterns both corresponding in the HighScore Plus phase database to mordenite zeolite.

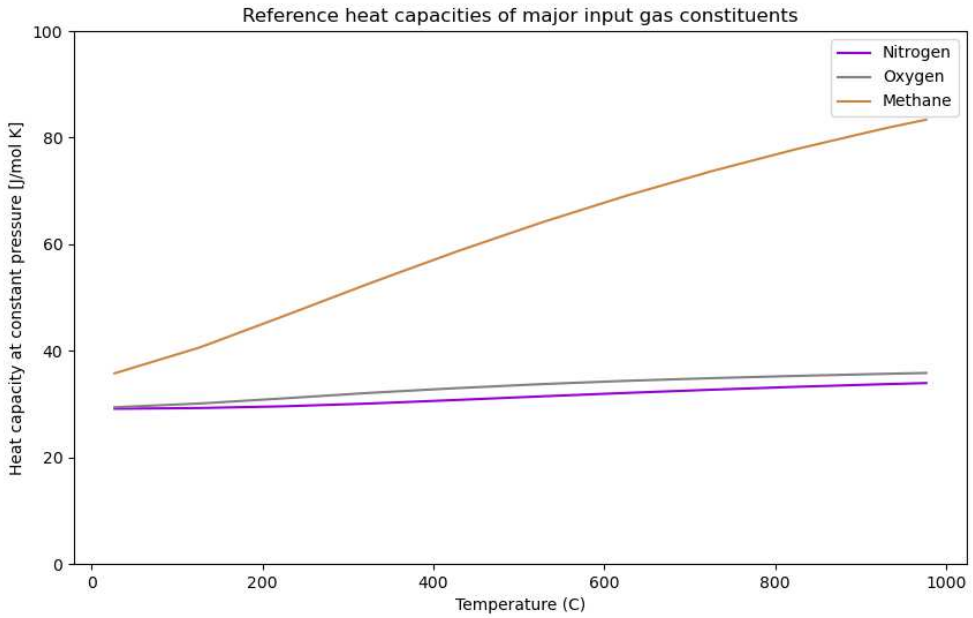

Figure 6-2: NIST reference values of the molar heat capacities of the major constituents of the input gas mixture [38]. While methane's heat capacity changes significantly under the temperature range, the change in heat capacity of nitrogen and oxygen is relatively small, resulting in a modest change in gas mixture heat capacity; the difference in gas mixture heat capacity from 20-400 °C at 1.4% methane was 25.1%.

Bibliography

[1] Myhre *et al.*, "Anthropogenic and natural radiative forcing," *Climate Change 2013: The Physical Science Basis. Contribution of Working Group I to the Fifth Assessment Report of the Intergovernmental Panel on Climate Change*, 2013.

[2] U. E. P. Agency, "Importance of methane," Jun 2022.

[3] Lee *et al.*, "Summary for policymakers," *Synthesis Report of the Intergovernmental Panel on Climate Change Sixth Assessment Report*, 2023.

[4] R. B. Jackson, S. Abernethy, J. G. Canadell, M. Cargnello, S. J. Davis, S. Féron, S. Fuss, A. J. Heyer, C. Hong, C. D. Jones, *et al.*, "Atmospheric methane removal: a research agenda," *Philosophical Transactions of the Royal Society A*, vol. 379, no. 2210, p. 20200454, 2021.

[5] A. I. Olivos-Suarez, À. Szécsényi, E. J. Hensen, J. Ruiz-Martinez, E. A. Pidko, and J. Gascon, "Strategies for the direct catalytic valorization of methane using heterogeneous catalysis: challenges and opportunities," *Acs Catalysis*, vol. 6, no. 5, pp. 2965–2981, 2016.

[6] Z. Zhu, W. Guo, Y. Zhang, C. Pan, J. Xu, Y. Zhu, and Y. Lou, "Research progress on methane conversion coupling photocatalysis and thermocatalysis," *Carbon Energy*, vol. 3, no. 4, pp. 519–540, 2021.

[7] Shindell *et al.*, "Global methane assessment: 2030 baseline report," *United Nations Environment Programme*, 2022.

[8] R. J. Brenneis, E. P. Johnson, W. Shi, and D. L. Plata, "Atmospheric-and low-level methane abatement via an earth-abundant catalyst," *ACS Environmental Au*, vol. 2, no. 3, pp. 223–231, 2021.

[9] T. Smith and J. Murrell, "Methanotrophy/methane oxidation," in *Encyclopedia of Microbiology (Third Edition)* (M. Schaechter, ed.), pp. 293–298, Oxford: Academic Press, third edition ed., 2009.

[10] K. T. Dinh, M. M. Sullivan, P. Serna, R. J. Meyer, M. Dincă, and Y. Román-Leshkov, "Viewpoint on the partial oxidation of methane to methanol using cu- and fe-exchanged zeolites," 2018.

[11] L. López-Pérez, V. Zarubina, and I. Melián-Cabrera, "The brunauer–emmett–teller model on alumino-silicate mesoporous materials. how far is it from the true surface area?," *Microporous and Mesoporous Materials*, vol. 319, p. 111065, 2021.

[12] Y.-S. Bae, A. O. Yazaydın, and R. Q. Snurr, "Evaluation of the bet method for determining surface areas of mofs and zeolites that contain ultra-micropores," *Langmuir*, vol. 26, no. 8, pp. 5475–5483, 2010.

[13] N. Y. Kozin, A. Voskov, A. Khvan, and I. Uspenskaya, "Thermodynamic properties of synthetic zeolite–mordenite," *Thermochimica Acta*, vol. 688, p. 178600, 2020.

[14] M. M. Mohamed, "Heat capacities, phase transitions and structural properties of cation-exchanged h-mordenite zeolites," *Thermochimica Acta*, vol. 372, no. 1, pp. 75–83, 2001.

[15] G. Johnson, I. Tasker, H. Flotow, P. O'Hare, and W. Wise, "Thermodynamic studies of mordenite, dehydrated mordenite, and gibbsite," *American Mineralogist*, vol. 77, no. 1-2, pp. 85–93, 1992.

[16] M. G. Shelyapina, E. A. Krylova, Y. M. Zhukov, I. A. Zvereva, I. Rodriguez-Iznaga, V. Petranovskii, and S. Fuentes-Moyado, "Comprehensive analysis of the copper exchange implemented in ammonia and protonated forms of mordenite using microwave and conventional methods," *Molecules*, vol. 24, no. 23, p. 4216, 2019.

[17] P. C. Bruzzese, E. Salvadori, S. Jäger, M. Hartmann, B. Civalleri, A. Pöppl, and M. Chiesa, "17o-epr determination of the structure and dynamics of copper single-metal sites in zeolites," *Nature Communications*, vol. 12, no. 1, p. 4638, 2021.

[18] Badische Anilin und Sodafabrik, "Copper chabazite: A milestone on the road to clean diesel engines," 2023. https://www.basf.com/us/en/who-we-are/innovation/our-innovations/copper-chabazite.html.

[19] I. Lezcano-Gonzalez, U. Deka, H. van der Bij, P. Paalanen, B. Arstad, B. Weckhuysen, and A. Beale, "Chemical deactivation of cu-ssz-13 ammonia selective catalytic reduction (nh3-scr) systems," *Applied Catalysis B: Environmental*, vol. 154-155, pp. 339–349, 2014.

[20] M. Iwamoto, H. Furukawa, Y. Mine, F. Uemura, S.-i. Mikuriya, and S. Kagawa, "Copper (ii) ion-exchanged zsm-5 zeolites as highly active catalysts for direct

and continuous decomposition of nitrogen monoxide," *Journal of the Chemical Society, Chemical Communications*, no. 16, pp. 1272–1273, 1986.

[21] S. Sato, Y. Yu-u, H. Yahiro, N. Mizuno, and M. Iwamoto, "Cu-zsm-5 zeolite as highly active catalyst for removal of nitrogen monoxide from emission of diesel engines," *Applied catalysis*, vol. 70, no. 1, pp. L1–L5, 1991.

[22] M. Colombo, I. Nova, and E. Tronconi, "A comparative study of the nh3-scr reactions over a cu-zeolite and a fe-zeolite catalyst," *Catalysis Today*, vol. 151, no. 3-4, pp. 223–230, 2010.

[23] A. Primo and H. Garcia, "Zeolites as catalysts in oil refining," *Chemical Society Reviews*, vol. 43, no. 22, pp. 7548–7561, 2014.

[24] M. A. Newton, A. J. Knorpp, V. L. Sushkevich, D. Palagin, and J. A. Van Bokhoven, "Active sites and mechanisms in the direct conversion of methane to methanol using cu in zeolitic hosts: a critical examination," *Chemical Society Reviews*, vol. 49, no. 5, pp. 1449–1486, 2020.

[25] D. K. Pappas, A. Martini, M. Dyballa, K. Kvande, S. Teketel, K. A. Lomachenko, R. Baran, P. Glatzel, B. Arstad, G. Berlier, *et al.*, "The nuclearity of the active site for methane to methanol conversion in cu-mordenite: a quantitative assessment," *Journal of the American Chemical Society*, vol. 140, no. 45, pp. 15270–15278, 2018.

[26] M. A. Newton, A. J. Knorpp, A. B. Pinar, V. L. Sushkevich, D. Palagin, and J. A. Van Bokhoven, "On the mechanism underlying the direct conversion of methane to methanol by copper hosted in zeolites; braiding cu k-edge xanes and reactivity studies," *Journal of the American Chemical Society*, vol. 140, no. 32, pp. 10090–10093, 2018.

[27] M. Guisnet and F. R. a Ribeiro, "Deactivation and regeneration of zeolite catalysts," 2011.

[28] S. Bhatia, J. Beltramini, and D. Do, "Deactivation of zeolite catalysts," *Catalysis Reviews—Science and Engineering*, vol. 31, no. 4, pp. 431–480, 1989.

[29] H. Taniguchi, T. Masuda, K. Tsutsumi, and H. Takahashi, "Direct measurement of the interaction energy between solids and gases. iii. comparison of the calorimetric titration method with the amine titration method for the determination of acid strength distribution of silica-alumina surface," *Bulletin of the Chemical Society of Japan*, vol. 51, no. 7, pp. 1970–1972, 1978.

[30] J. S. Tumuluru, J. R. Hess, R. D. Boardman, C. T. Wright, and T. L. Westover, "Formulation, pretreatment, and densification options to improve biomass specifications for co-firing high percentages with coal," *Industrial biotechnology*, vol. 8, no. 3, pp. 113–132, 2012.

[31] S.-w. Ham, H. Choi, I.-S. Nam, and Y. G. Kim, "Deactivation of copper-ion-exchanged hydrogen-mordenite-type zeolite catalyst by so2 for no reduction by nh3," *Catalysis today*, vol. 11, no. 4, pp. 611–621, 1992.

[32] D. Adanenche, A. Aliyu, A. Atta, and B. El-Yakubu, "Residue fluid catalytic cracking: A review on the mitigation strategies of metal poisoning of rfcc catalyst using metal passivators/traps," *Fuel*, vol. 343, p. 127894, 2023.

[33] K. Ding, A. Gulec, A. M. Johnson, T. L. Drake, W. Wu, Y. Lin, E. Weitz, L. D. Marks, and P. C. Stair, "Highly efficient activation, regeneration, and active site identification of oxide-based olefin metathesis catalysts," *ACS Catalysis*, vol. 6, no. 9, pp. 5740–5746, 2016.

[34] M. M. Yung, A. K. Starace, M. B. Griffin, J. D. Wells, R. E. Patalano, K. R. Smith, and J. A. Schaidle, "Restoring zsm-5 performance for catalytic fast pyrolysis of biomass: Effect of regeneration temperature," *Catalysis Today*, vol. 323, pp. 76–85, 2019.

[35] A. Aguinaga and M. Montes, "Regeneration of a nickel/silica catalyst poisoned by thiophene," *Applied Catalysis A: General*, vol. 90, no. 2, pp. 131–144, 1992.

[36] M. Guisnet, L. Costa, and F. R. Ribeiro, "Prevention of zeolite deactivation by coking," *Journal of Molecular Catalysis A: Chemical*, vol. 305, no. 1-2, pp. 69–83, 2009.

[37] "Delayed coking," *Jonell Systems Filtration Group*, 2023.

[38] National Institute of Standards and Technology, "Nist chemistry webbook, srd 69," 2023.

[39] X. Wang, F. Zhou, Y. Ling, Y. Xiao, B. Ma, X. Ma, S. Yu, H. Liu, K. Wei, and J. Kang, "Overview and outlook on utilization technologies of low-concentration coal mine methane," *Energy & Fuels*, vol. 35, no. 19, pp. 15398–15423, 2021.

[40] P. R. D'Urso, C. Arcidiacono, and G. Cascone, "Uncertainty in determining ammonia and methane emissions at different sampling locations in an open-sided dairy barn," pp. 145–150, 2021.

[41] M. N. Hayek and S. M. Miller, "Underestimates of methane from intensively raised animals could undermine goals of sustainable development," *Environmental Research Letters*, vol. 16, no. 6, p. 063006, 2021.

[42] J. J. Owen and W. L. Silver, "Greenhouse gas emissions from dairy manure management: a review of field-based studies," *Global change biology*, vol. 21, no. 2, pp. 550–565, 2015.

[43] S. Bakkaloglu, J. Cooper, and A. Hawkes, "Methane emissions along biomethane and biogas supply chains are underestimated," *One Earth*, vol. 5, no. 6, pp. 724–736, 2022.

[44] H. Baldé, A. C. VanderZaag, S. Burtt, L. Evans, C. Wagner-Riddle, R. L. Desjardins, and J. D. MacDonald, "Measured versus modeled methane emissions from separated liquid dairy manure show large model underestimates," *Agriculture, Ecosystems & Environment*, vol. 230, pp. 261–270, 2016.

[45] T. Howard, "University of texas study underestimates national methane emissions at natural gas production sites due to instrument sensor failure," *Energy Science & Engineering*, vol. 3, no. 5, pp. 443–455, 2015.

[46] S. N. Riddick and D. L. Mauzerall, "Likely substantial underestimation of reported methane emissions from united kingdom upstream oil and gas activities," *Energy & Environmental Science*, vol. 16, no. 1, pp. 295–304, 2023.

[47] N. Kholod, M. Evans, R. C. Pilcher, V. Roshchanka, F. Ruiz, M. Coté, and R. Collings, "Global methane emissions from coal mining to continue growing even with declining coal production," *Journal of Cleaner Production*, vol. 256, p. 120489, 2020.

[48] B. D. Jr, "Texas dairy farm explosion kills 18,000 cows," *British Broadcasting Corporation*, April 2023. https://www.bbc.com/news/world-us-canada-65258108.

[49] D. A. Brown, "Lessons learned from ipcc's underestimation of climate change impacts about the need for a precautionary climate change science," pp. 3–10, 2020.

[50] C.-H. Cheng and S. A. Redfern, "Impact of interannual and multidecadal trends on methane-climate feedbacks and sensitivity," *Nature communications*, vol. 13, no. 1, p. 3592, 2022.

[51] R. P. Allan, E. Hawkins, N. Bellouin, and B. Collins, "Ipcc, 2021: summary for policymakers," 2021.

[52] U. D. of Energy, "Department of energy invests $47 million to reduce methane emissions from oil and gas sector," March 2023.

[53] U. D. of Energy, "Department of energy invests more than $130 million to lower nation's carbon pollution," January 2023.

[54] Shindell *et al.*, "Global methane assessment: Benefits and costs of mitigating methane emissions," *United Nations Environment Programme, Climate & Clean Air Coalition*, 2021.

[55] M. Begon, R. W. Howarth, and C. R. Townsend, *Essentials of ecology*. Wiley Hoboken, 2014.